Supporting Information for:

The Fusion Peptide of SARS-CoV-2 Spike Rearranges into a Wedge Inserted in Bilayered Micelles

Rama K. Koppisetti[1], Yan G. Fulcher[1], and Steven R. Van Doren*[1,2]

[1] Dept. of Biochemistry, University of Missouri, Columbia, MO 65211 USA

[2] Institute for Data Science and Informatics, University of Missouri, Columbia, MO 65211 USA

Methods

Recombinant expression and labeling of the fusion peptide of SARS-CoV-2

The 42 residues at the mature N-terminus of the S_2 subunit of SARS-CoV-2 Spike span from conserved Ser816 at the S_2' site of proteolysis through conserved Gly857. This corresponds to the Ser816 - Asn856 demonstrated to be the bona fide, functional fusion peptide (FP)[1,2]. The UniProtKB accession number is P0DTC2, and its processed chain PRO_0000449649. The PFAM accession number is PF01601. A recombinant fusion protein was expressed with N-terminal His tag through the B1 domain of protein G, and TEV protease cleavage site followed by the FP sequence from Ser816 through Gly857. The coding sequence constructed is illustrated in Fig. S1 in Supporting Information. An internal substitution of I844V removed a methylene group from this GB1 – FP construct. IDT (Coralville, Iowa) synthesized this region with codons optimized for expression in *E. coli* (Fig. S1). The duplex DNA was digested by Nde I and EcoR1 and subcloned into the pET27b(+) expression plasmid.

The GB1 fusion with FP was expressed in *E. coli* gold BL21(DE3) RIL harboring this plasmid. Labeling with stable isotopes of ^{15}N or ^{15}N or ^{13}C for NMR spectroscopy expressed the GB-FP fusion from this host in PG minimal media using $^{15}NH_4Cl$ as the nitrogen source and D-glucose uniformly labeled with ^{13}C as carbon source [3]. Expression was induced in 500 ml of culture in early log phase (OD_{600} near 0.6 - 0.8) using a final concentration of 0.5 mM IPTG. Growth and expression were continued for 6 to 8 hrs. at 37^{o}C. The GB1 - FP protein was observed in inclusion bodies after lysis and centrifugation of the *E. coli* culture using a Branson sonicator. The pellet containing inclusion bodies, occupying two centrifuge tubes, was solubilized with 12.6 g of urea in 17 ml of buffer of 20 mM Tris-HCl (pH 8.0) in each tube. After centrifugation, the soluble fraction containing soluble, denatured GB1 – FP was retained for isolation of FP.

Protein purification

The denatured GB1 – FP was loaded onto a column of nitrilotriacetic acid (NTA; GenScript) equilibrated with 20 mM Tris-HCl (pH 8.0) and 6M urea at room temperature. After thoroughly washing with several column volumes of 20 mM imidazole (pH 8.0), pure denatured GB1 – FP was eluted with 300 mM imidazole (pH 8.0). Dithiothreitol was then added to 5 mM to reduce disulfide bonds. Denatured GB1 – FP was diluted to 0.1 mg/ml for refolding. Overnight refolding was conducted by dialyzing against 20 mM Tris-HCl (pH 8.0), 3.0 mM cysteine (reduced), 0.3 mM

cystine (oxidized), followed by another round of dialysis vs. 20 mM Tris-HCl (pH 8.0) omitting the cysteine and cystine to allow full oxidation of Cys840 and Cys851 and formation of a disulfide crosslink between them. The folded GB1 – FP was concentrated to 1 to 2 ml. 150 units of tobacco etch virus (TEV) protease (New England Biolabs) was added, mixed gently, and incubated at 4°C for at least 36 h. Upon completion of proteolysis by TEV, judged by the appearance of the GB1 and FP bands by SDS-PAGE, the sample was loaded onto an NTA column (2 ml) removing the His-tagged GB1 protein while the SARS-2 fusion peptide (FP) flow through the NTA resin equilibrated in 20 mM imidazole (pH 8.0). The FP-containing fraction was loaded onto a Q-Sepharose column (2 ml) equilibrated in 20mM Tris-HCl (pH 8.0) to remove proteolytic fragments of FP. The pure, refolded FP was eluted with 20mM Tris-HCl (pH 8.0), 1 M NaCl and dialyzed into 20 mM Tris-acetate (pH 5.0). Samples used for NMR spectroscopy were concentrated further. The homogeneity and molecular weight corresponding to the Ser816 – Gly857 region were established by LC-MS. The separation used a reversed-phase C4 column, i.e. an XBridge Protein BEH C4, 300Å, 3.5 µm, 4.6 mm X 150 mm from Waters (Milford, MA) with a 168 diode array detector, a 507e autoinjector and the 32 KARAT software package (Gold System from Beckmann Coulter, Fullerton, CA). This HPLC system was coupled with an LCQ Fleet ion trap mass spectrometer (Thermo Fisher, Waltham, MA).

Assays of the disulfide crosslink

The formation of the disulfide crosslink was determined by mass spectrometry, loss of thiol reactivity, and ^{13}C chemical shifts. The disulfide crosslink was confirmed routinely by the mass data from aforementioned LC-MS protocol performed in the Molecular Interactions Core. The lack of reactive thiols was determined using Ellman's reagent (5,5-dithio-bis-(2-nitrobenzoic acid), DTNB) assayed spectrophotometrically. The large downfield of the $^{13}C\beta$ chemical shifts of Cys840 and Cys851 to 39.8 or 38.7 ppm, respectively, confirmed the disulfide. Additional confirmation of the disulfide crosslink came from MS/MS of tryptic peptides: The fusion peptide was digested in trypsin (Promega) and characterized by LC-MS and MS/MS using an LTQ Orbitrap FT-MS in the Gehrke Proteomics Core. The tryptic peptides were enriched with a C8 trap column (Thermo Fisher, µ-precolumn – 300 µm i.d. x 5 mm, C8 Pepmap 100, 5 µm, 100 Å). Bound peptides were eluted onto a 11cm, 75µm i.d. pulled-needle analytical column packed with HxSIL C18 reversed phase resin (Hamilton) and eluted with a gradient of increasing acetonitrile at 400 nL/min using a Proxeon Easy nLC system attached to the LTQ Orbitrap mass spectrometer. FT-MS data were collected at resolution of 30,000 with 300-1800m/z profile. In each cycle the nine most abundant peptides were selected for MS-MS with 2m/z mass window. Thermo Xcalibur RAW data files were converted to MGF files using MassMatrix software and analyzed on our Mascot server (v. 2.5.1). Data files were searched against the Swissprot database or NCBI-Viruses using the parameters of trypsin, 20 ppm mass error on precursor, and 0.6 Da mass error on fragments.The MS/MS spectra were viewed using Qual Browser.

Choice of conditions for solution NMR

pH 5.0 was chosen for mimicking the endosomal pathway of cell entry by coronaviruses [4]. The I844V mutation improved solubility and homogeneity compared to that from appending a solubility-enhancing tag to the C-terminus (GGGKKKK) akin to that of previous reports [1,5]. Importantly, I844V increased the short lifetimes in membrane mimics from about 20 to 40 hours for the wild-type FP to 4 to 8 days for FP(I844V).

Sufficient rotational diffusion is required for good NMR spectra in solution. So we chose the smallest disk-shaped membrane mimics that retain at least partial bilayer character, namely bilayered micelles composed of one long-chain phospholipid per two short-chain phospholipids,

i.e., 1 DMPC per 2 DHPC (q=0.5)[6–8]. However, we replaced DHPC with hexanoyl fatty acyl chains by DH[7]PC with heptanoyl fatty acyl chains which have the advantage of decreasing the critical micelle concentration (CMC) to ~1 mM [9]. The smaller CMC results in fewer detergent-like monomers to complicate the sample and experiments. Concentrated DMPC:DH[7]PC (1 M total lipid; see preparation below) were mixed with concentrated FP to arrive at a final total [lipid] of 180 mM. Temperatures above the phase transition of DMPC, particularly 32°C, sharpened the lines to complete the ^{15}N TROSY spectra of FP in DMPC:DH[7]PC bicelles (q=0.5).

Preparation of concentrated DMPC:DH[7]PC bicelles

Concentrated stock solutions of bicelles with 1 M total lipid, composed of one DMPC per DH[7]PC molecule (q=0.5), were prepared as follows. 180 mg of DH[7]PC (Avanti Polar Lipids) was dissolved in chloroform for transfer of the DH[7]PC. The chloroform was evaporated under a stream of argon gas, followed by drying under vacuum for 60 h. 200 mg of DMPC was added to 10 ml of 20 mM Tris-acetate (pH 5.0) and allowed to hydrate for 2 h at 42 °C with occasional vortex mixing of the suspension. The homogeneity of the DMPC suspension was improved using three freeze-thaw cycles and three cycles of sonication for 10 to 15 min in a bath sonicator (Laboratory Supplies Co., Hicksville, NY). The milky white suspension became translucent with a blue tint during incubation at 42 °C for 1 h. The DMPC vesicles were concentrated by microcentrifugation for 30 min at 20 °C to collect the large unilamellar vesicles (LUVs) and multilamellar vesicles (MLVs), comprising 90% of the vesicles, while losing the 10% which were small unilamellar vesicles in the supernatant. 350 µl of your 20mM Tris-acetate (pH 5.0) was added to the DH[7]PC and hydrated at 42 °C for 1 h. The concentrated LUVs and MLVs of DMPC were dissolved in the DH[7]PC solution and incubated at 42 °C until an even suspension formed in 1 to 2 h. The suspension was frozen by plunging into liquid nitrogen. The suspension was subjected to two more cycles of thawing at 42 °C and freezing in liquid nitrogen before freezing small aliquots with liquid nitrogen for storage at -80 °C until use. The ratio of 1 DMPC to 2 DH[7]PC was verified from the 1:2 ratio of their respective methyl peak areas in the 1H NMR spectrum.

Triple resonance NMR spectroscopy

Due to limited sample lifetimes, non-uniform sampling (NUS)[10,11] was used in acquiring most spectra rapidly using a Bruker Avance III NMR spectrometer with 5 mm TCI cryoprobe. Processing of NUS spectra employed the compressed sensing option of matrix decomposition (MDD) software[12,13]. The triple resonance spectra of the backbone[14–16] used were 3D HNCACB, CBCA(CO)NH, HNCO and HN(CA)CO spectra. A combination of H(CCO)NH, (H)CC(CO)NH[17,18] and adiabatic HCCH-TOCSY spectra[19] were used to assign aliphatic sidechains. The aromatic sidechains were assigned using (Hb)Cb(CgCd)Hd and (Hb)Cb(CgCd)He spectra[20]. ^{15}N-separated, ^{13}C-separated, and simultaneously ^{13}C/^{15}N-separated NOESY[21] spectra used 120 msec mixing times. An aromatic ^{13}C TROSY-edited NOESY[22] used a 140 msec mixing time.

NMR spectral and relaxation calculations

Radial shifts of NMR peaks were calculated per Pythagoras' rule, but with scaling of the ^{15}N spectral range to the ^{1}H range:

$$\Delta\omega_{HN} = \sqrt{(\Delta\omega_H)^2 + (\Delta\omega_N/5)^2} \qquad eq.S1$$

Scores of the secondary structural propensity (SSP) were calculated using ^{13}Cα and ^{13}Cβ shifts [23]. Helix exhibits positive SSP scores as large as 1.0, while extended structure, including β-strands, exhibit negative SSP scores as small as -1.0.

Reduced spectral densities of backbone amide fluctuations were calculated from ^{15}N R_1 and R_2 relaxation series collected in triplicate and $^{15}N\{^1H\}$ NOE difference spectra at NMR spectral frequencies of zero (filled squares), ^{15}N (half-filled circles, 81 MHz), and ^1H (open triangles, 800 MHz * 0.87) [24–26]. The mean ratio of ^{15}N R_2/R_1 provides an estimate of the rotational correlation time of diffusion from this expression[27]:

$$\tau_c = \frac{1}{2\omega_c}\sqrt{\frac{6R_2}{R_1} - 7} \qquad eq.S2$$

Measurement of PREs between amide groups and 14-doxyl PC

Bicelles comprising 1 DMPC: 2 DH^7PC (q=0.5) were added to ^{15}N labeled fusion peptide (250μM final concentration) to a total phospholipid concentration of 150 mM, i.e. 50 mM of DMPC and 100 mM DH^7PC. and. An ^{15}N HSQC modified to incorporate an 8 ms CPMG train that suppresses ^1H-^1H J-couplings[28] was used to collect spectra without and with addition of a spin-labeled lipid [29]. PREs were introduced by adding 16:0-14 doxyl PC (1-palmitoyl-2-stearoyl-14-doxyl-sn-glycero-3-phosphocholine; Avanti Polar Lipids, Alabaster, AL) to 770uM, which is about one spin-labeled molecule per leaflet of the bicelle molecule.

NMR structure determination

NOEs from ^{15}N- and aliphatic ^{13}C-separated NOESY spectra (120 ms mixing) and aromatic ^3C-separated NOESY (140 ms mixing) were assigned manually for judicious decisions in crowded regions of the spectra, especially the methyl region. Approximately 191 NOEs were assigned manually in an iterative approach. Structures were calculated using CYANA 3.0 software with unambiguous restraints converted into distance estimates with 3 to 5 Å upper bounds and 3 Å pseudo atom corrections for pairs of methyl groups and aromatic groups. Of 50 structures retained from the calculation in CYANA, the 20 lowest energy models (lowest target function) were selected and subjected to brief steepest descents energy minimization (110 – 125 steps) positional restraints in Gromacs 2018 using the CHARMM27 forcefield at 283 K until energies dropped to ≤ 2800 kJ/mol/nm. The five models with lingering violations of bond angles were removed from the ensemble. Table S1 and S2 refer to the NMR restraints, violation analysis, and structural quality statistics for the ensemble of 15 structures deposited in RCSB (accession code 7MY8).

Supporting Figures

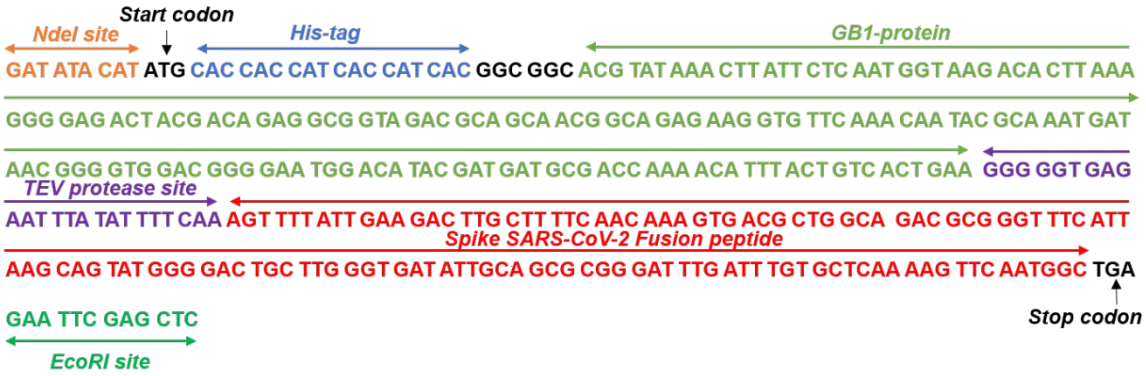

Figure S1. Gene fusion of the B1 domain of protein G with the fusion peptide SARS2-CoV-2 synthesized for recombinant expression. The coding strand is color- coded by the restriction sites and portions of the open reading frame for six-His tag, protein G B1, site for TEV proteolysis, and the 42 codons of the fusion peptide. IDT optimized the codon usage for expression in *E. coli*. The substitution for I844V replaces the ATT of the 29th codon of the fusion peptide with GTT.

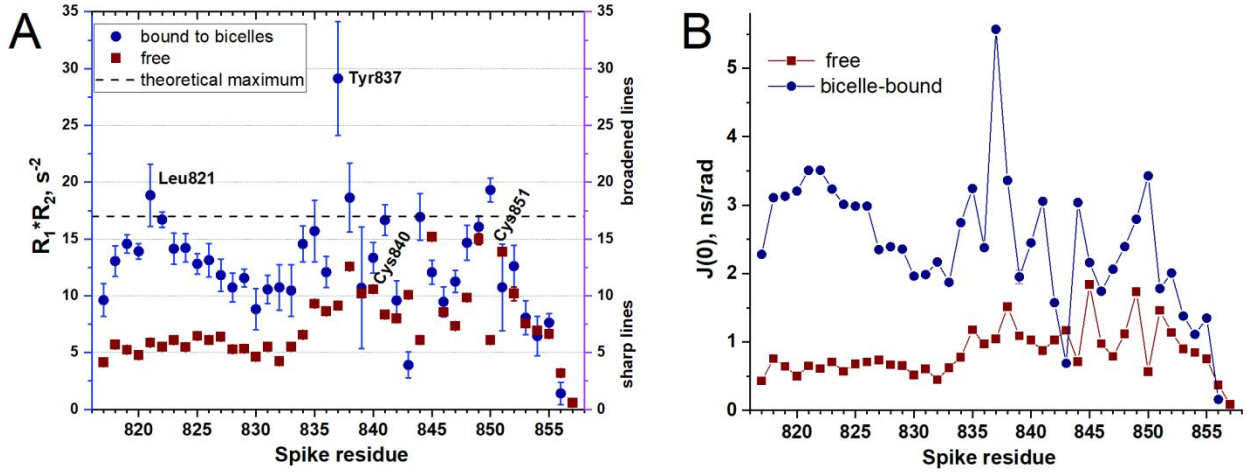

Figure S2. ^{15}N NMR relaxation of the fusion peptide of SARS-CoV-2(I844V) indicates intrinsic disorder in aqueous solution and ordering in bicelles. The free polypeptide is represented by red symbols and the state bound to bicelles (q=0.5) by blue symbols. The NMR spectra were measured at pH 5.0, 32 °C, and 800 MHz.

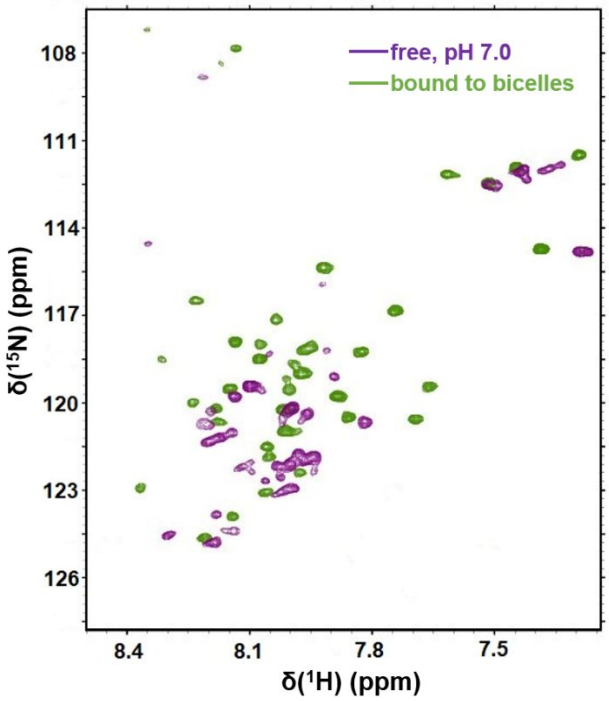

Figure S3. Evidence of disorder-to-order transition at pH 7 upon addition of bicelles. ^{15}N HSQC spectra SARS-2 FP(I844V) were acquired in 20 mM Tris-HCl (pH 7.0) at 32 °C at 800 MHz. Contours of the free state are purple and those in the presence of bicelles (q=0.5) are green. The final phospholipid concentration was 150 mM, comprising 50 mM DMPC and 100 mM DH^{7}PC. The fewer amide NMR peaks of the free state at pH 7 than at pH 5 are attributable to broadening by rapid exchange with solvent water.

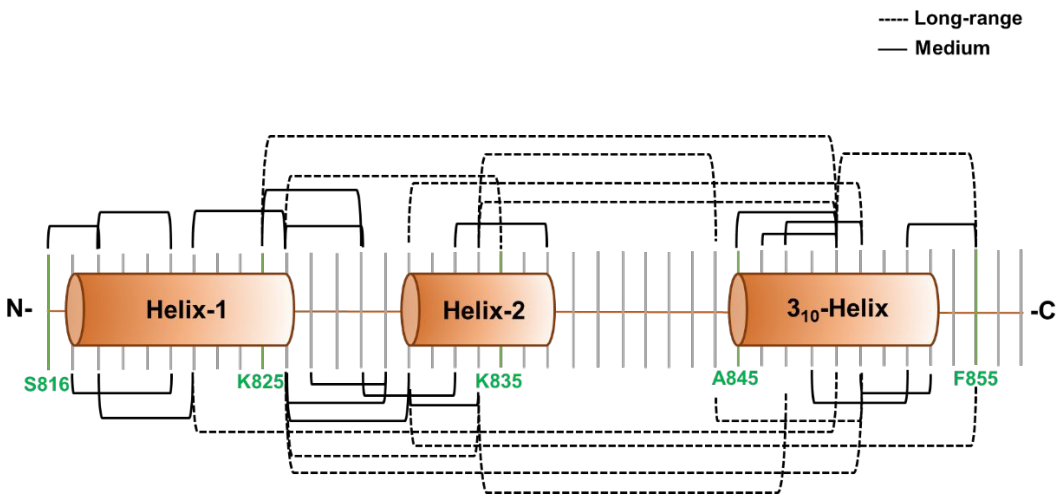

Figure S4. Distribution of long- and medium-range NOEs in SARS-2 FP in bicelles. The connectivity between two amino acids with dashed lines represents evidence of proximity from one or more long-range NOEs. Solid lines represent medium-range NOEs. These were assigned in 3D ^{13}C and ^{15}N-separated NOESY spectra.

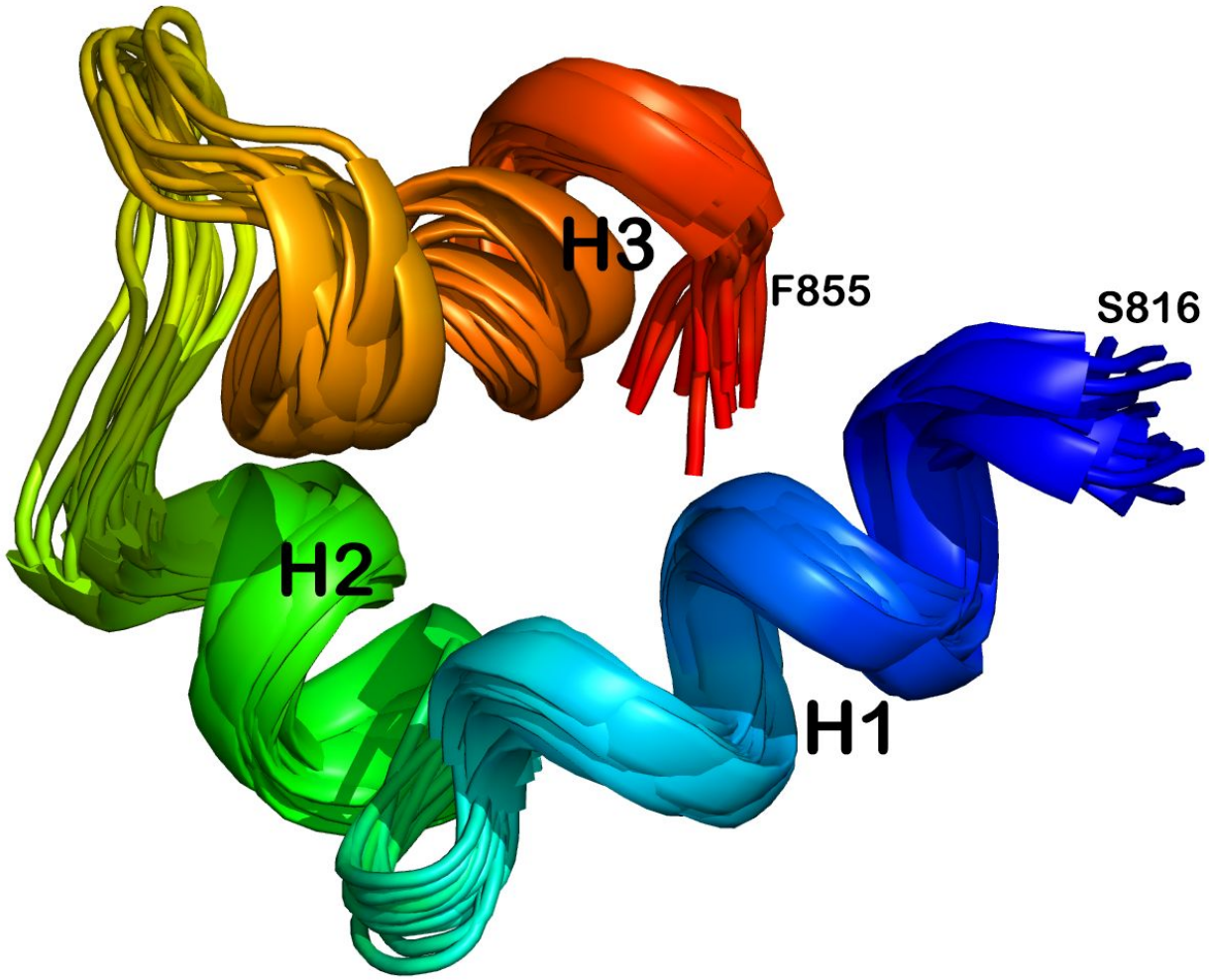

Figure S5. Bundle of 15 NMR structural models. The backbone ribbon of the ensemble (PDB: 7MY8) is colored by position in the chain. The structural statistics are listed in Tables S1 and S2.

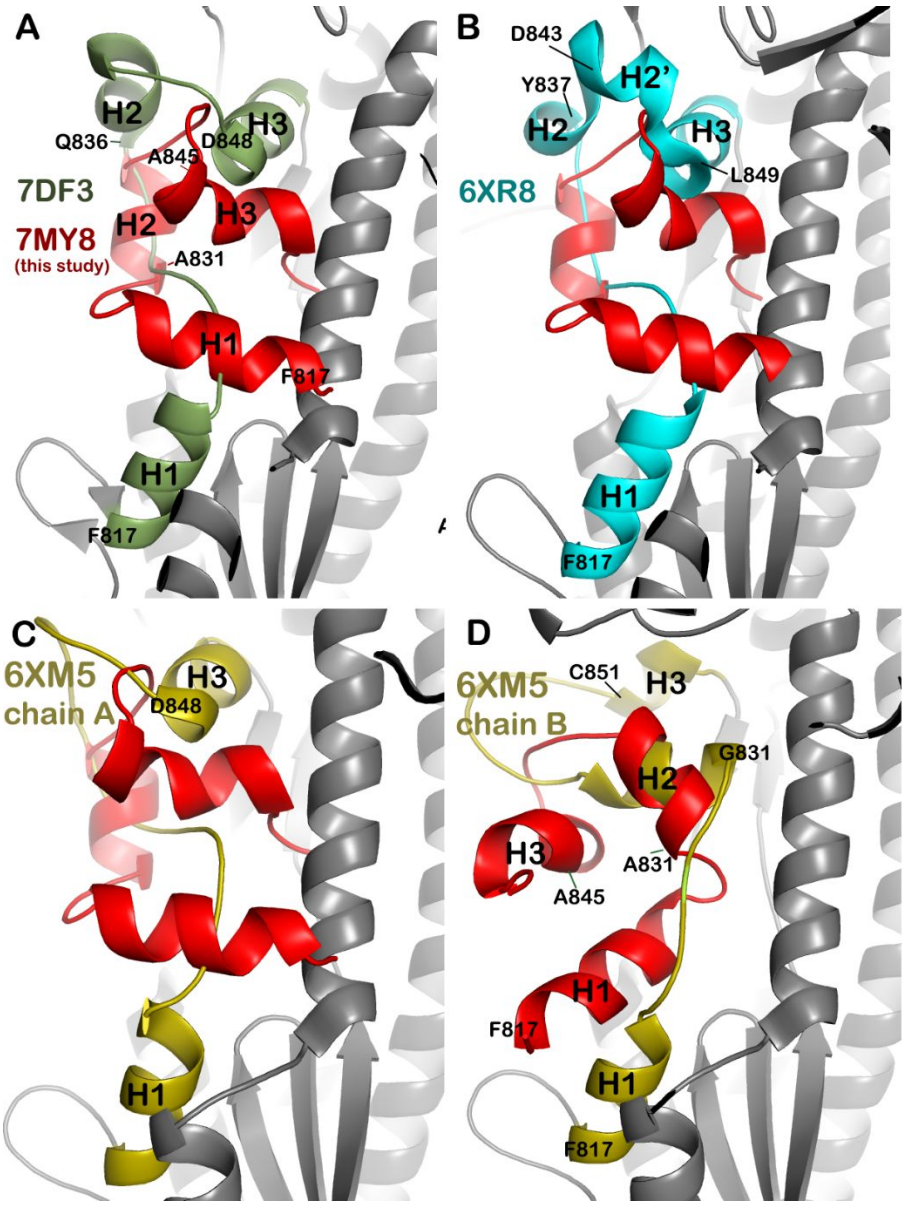

Figure S6. The closed, bicelle-inserted conformation of FP aligns poorly with the range of open conformations reported in the cryo-EM models of the tightly packed form of pre-fusion Spike in which all RBDs are down. The backbone ribbons of the structural models cryo-EM from cryo-EM are colored gray with green or cyan highlighting of the FP portion of the sequence reported by refs [1,2]. The ribbon of representative NMR structural model 2 of the bicelle-inserted form of FP (pH 5) is colored red. The first residue in the sequence of each helix is listed. Residues Phe817 through Gln853 of the NMR and tightly packed cryo-EM structural models were superposed providing backbone RMSD values of 9.2 to 10.5 Å in cases (A) – (D). The cryo-EM coordinates were reported by ref [30] (A) ref [31] (B), and ref [32] (C,D). The three protomers of 6XM5 differ from one another in conformations of the FP region. The structural alignments of (A - C) suggest the appearance of steric clashes of the termini of the bicelle-inserted state (red) with central helix (CH) of the prefusion S_2 subunit.

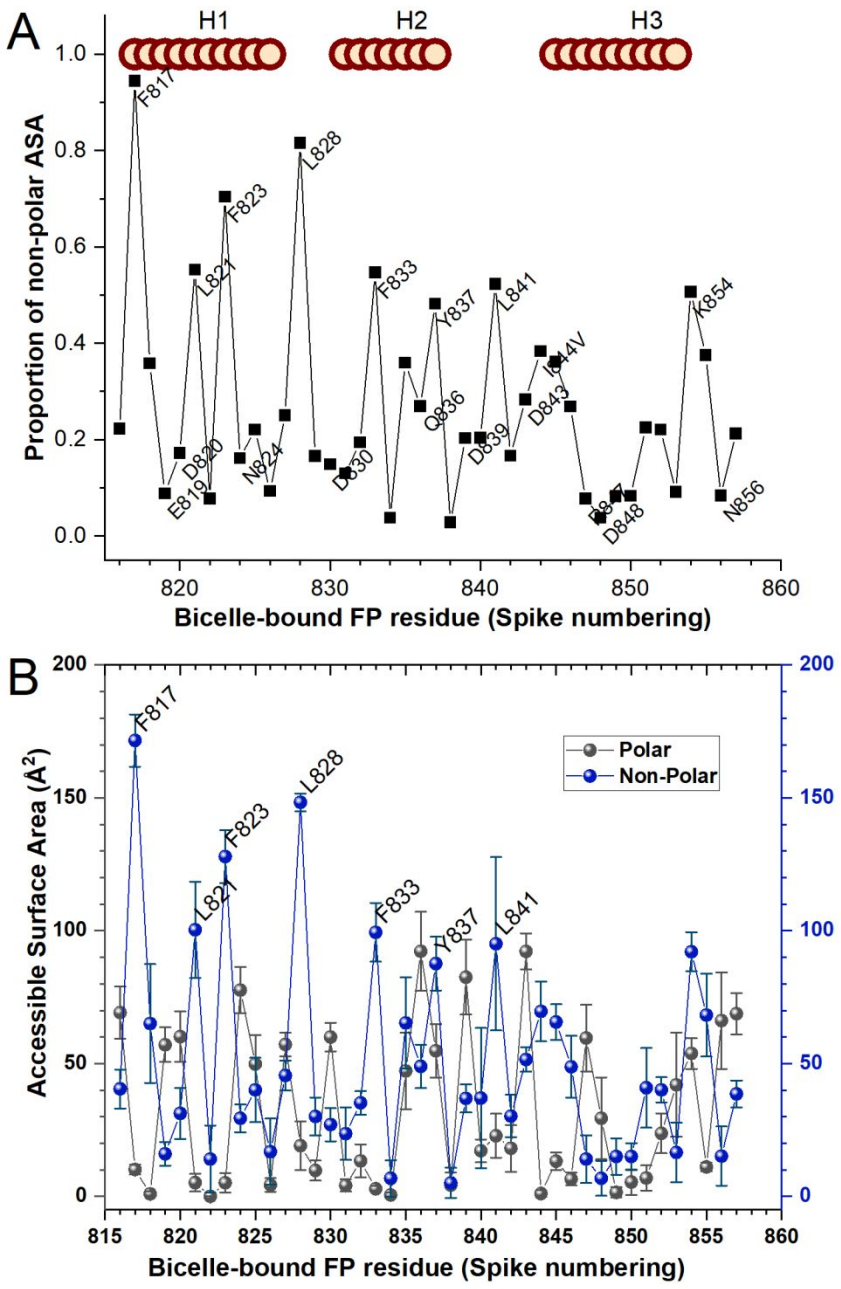

Figure S7. The accessible surface area (ASA) and its polarity of each residue of the bicelle-bound fusion peptide of SARS-CoV-2. Both the polar and non-polar components of the ASA of each residue were quantified using the program NACCESS 2.1.1 [33] for the top 6 models in the NMR structural ensemble. (A) The non-polar ASA of each residue is normalized by the total ASA of Phe817. (B) Both the polar and non-polar fractions of the ASA of each residue are plotted.

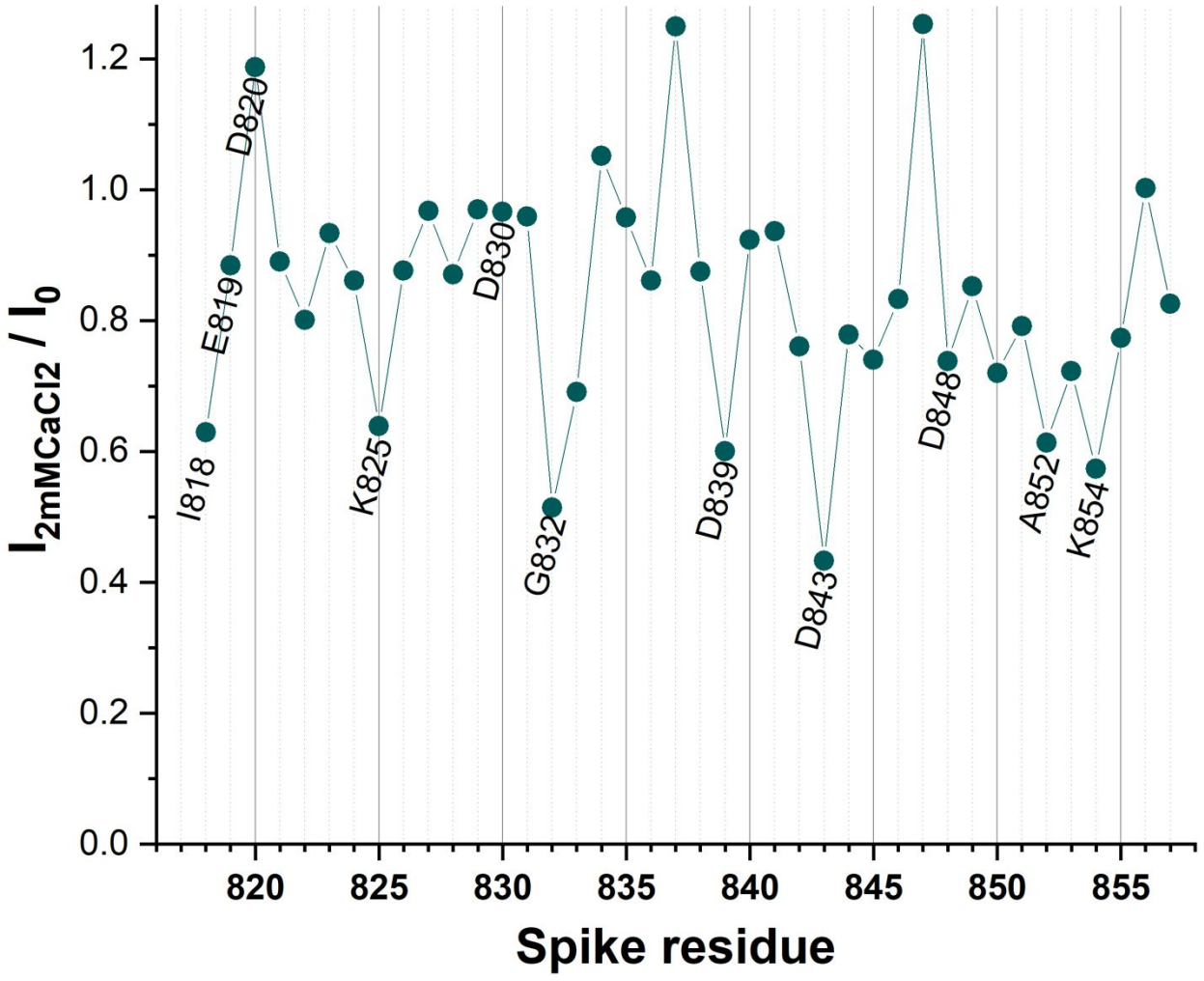

Figure S8. Broadening of backbone amide NMR peaks of FP in bicelles by addition of 2 mM $CaCl_2$. The spectra were acquired in 20 mM Tris-HCl (pH 7.0), 50 mM DMPC, and 100 mM DH^7PC at 32 °C at 800 MHz. Line broadening is implied by a smaller peak height after addition of 2 mM $CaCl_2$, $I_{2mM\ CaCl2}$, than before the addition, I_0.

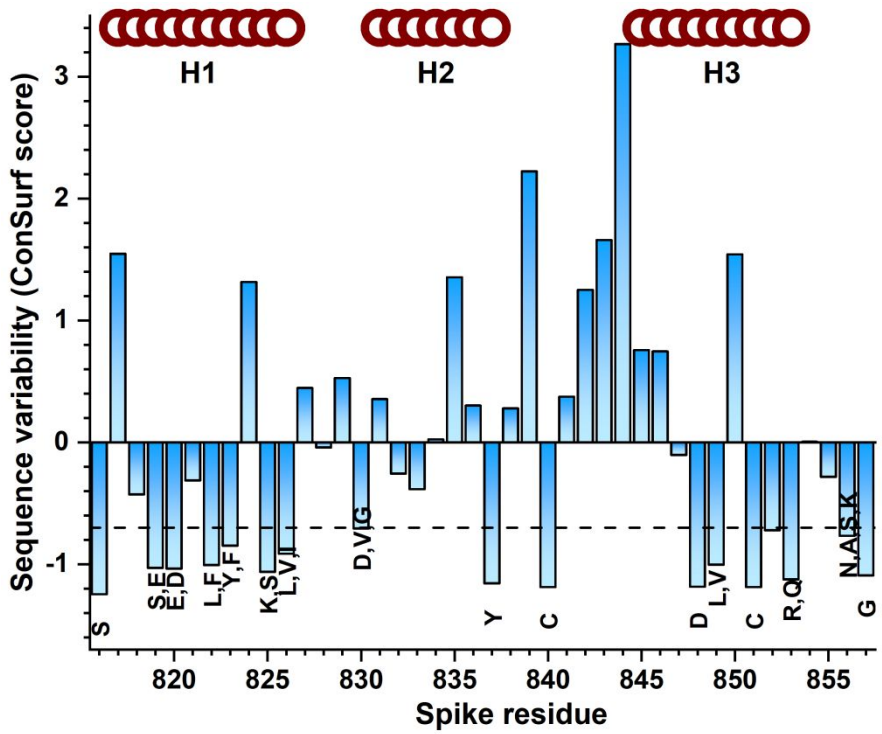

Figure S9. Amino acid conservation scores calculated by the ConSurf server upon a BLAST alignment of 45 diverse beta-coronaviral sequences.

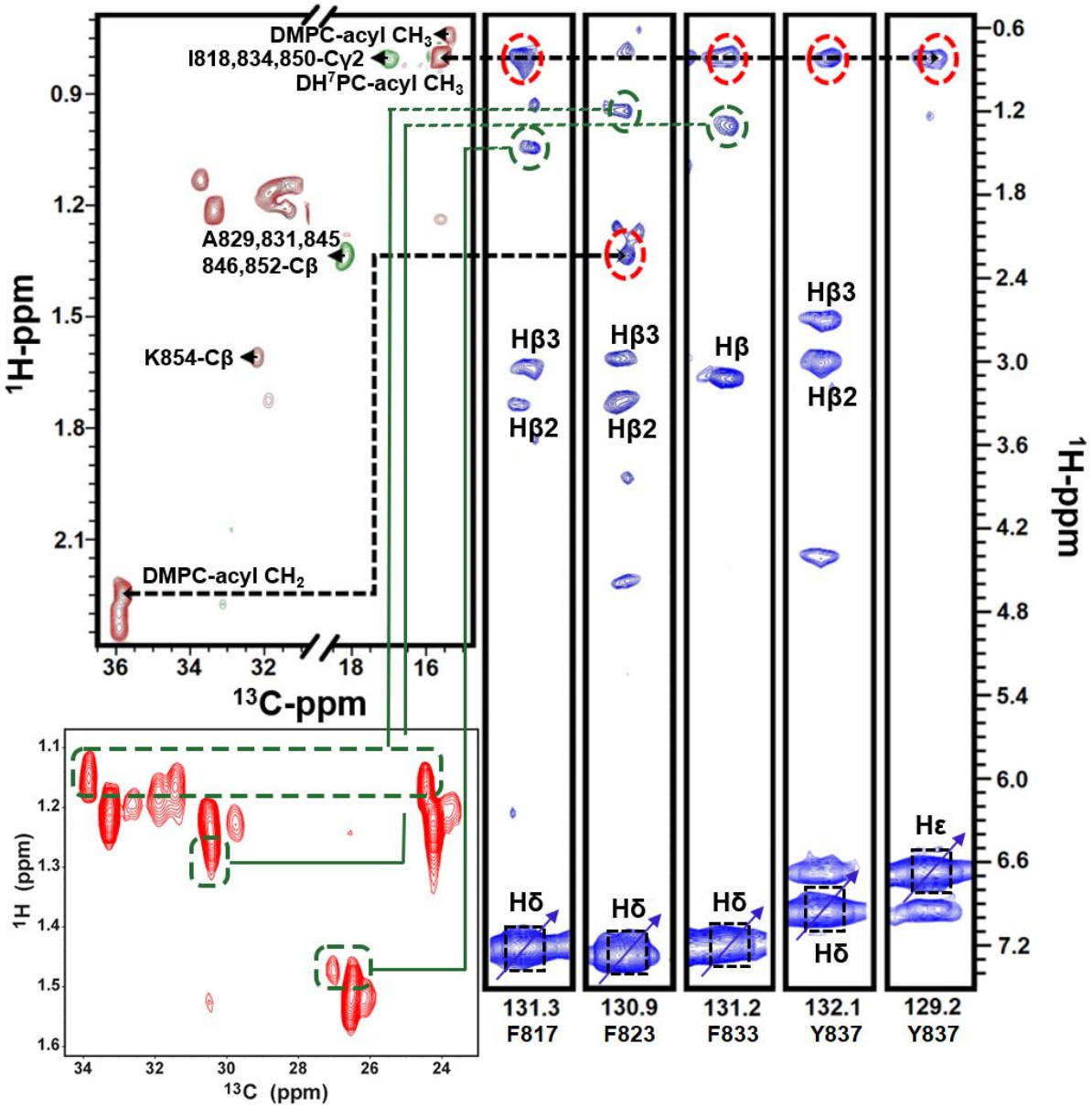

Figure S10. NOEs from fatty acyl chains in the bicelles to aromatic groups of helices 1 and 2. The left panels depict portions of the constant time ^{13}C-HSQC spectra of bicelles containing FP (upper left) and bicelles without FP (lower left). DH^{7}PC acyl CH_3 and DMPC acyl CH_2 peaks can be matched to NOEs (within red ellipses) to aromatic protons of Phe817, Phe823, Phe833, and Tyr837 detected in a 3D ^{13}C-separated NOESY-aromatic TROSY spectrum[34] shown in strips at right with blue contours. These three phenylalanine residues also have ambiguous NOEs to CH2 peaks unassigned in the interior of the acyl chains of the phospholipids, as indicated by green lines connected to candidate CH2 peaks of the CT-HSQC spectrum of bicelles.

Supporting Tables

Table S1. NMR Restraints used in structural calculations.

Distance Restraints:	
Inter-residue	192
Sequential NOEs (|i-j| = 1)	80
Medium range NOEs (1 < |i-j| ≤ 4)	86
Long range NOEs (|i-j| > 4)	26
Disulfide restraints	2
Dihedral Restraints:	
Total dihedral angle restraints	53
Φ	31
Ψ	22
Structural Statistics (mean ± SD)	
Violations (mean and s.d.)	
Distance constraints (Å)	0.19 ± 0.01
Dihedral constraints (°)	4.15 ± 0.82
Max. dihedral angle violation (°)	6.52
Max. distance constraints violation (Å)	0.44
Accession numbers at databases	
RCSB, structural coordinates and restraints	7MY8
BMRB, chemical shift assignments (I844V)	30909
BMRB, backbone amid shift assignments (WT)	50958

Table S2. Evaluation of NMR structural models.

Ramachandran analysis[1]	
Residues in the most Favored region (%)	88 ± 5%
Residues in Allowed region (%)	10 ± 5%
Residues in Outliers region (%)	2 ± 1%
PROCHECK G-factor (φ / ψ only)	-0.52
PROCHECK G-factor (all dihedrals)	-0.71
	RMSZ[2]
Bond lengths	1.54 ± 0.08 Å
Bond angles	1.95 ± 0.12°
Molprobity Validation[3]	
Clash score, all atoms	1.29 ± 1.34 (98.5 ± 1.5 percentile)
Molprobity score	1.75 ± 0.29 (84.5 ± 12.5 percentile)
Average pairwise r.m.s deviation to most representative structure (Å)[4]	
Backbone (residues 817-855)	0.90 ± 0.40
All heavy atoms (residues 817-855)	1.39 ± 0.56
No. of α-helixes	2
No. of 3_{10}-helixes	1
No. of β-strands	0
Location of α-helixes	F817-V826; A831-Y837
Location of 3_{10}-helix	A845-Q853

[1] from PROCHECK-NMR[35]

[2] RMSZ is the (average) root-mean-square of all Z-scores of the bond lengths (or angles).

[3] from Molprobity[36]

[4] The most representative NMR structural model is model 2.

Literature cited

(1) Lai, A. L.; Millet, J. K.; Daniel, S.; Freed, J. H.; Whittaker, G. R. The SARS-CoV Fusion Peptide Forms an Extended Bipartite Fusion Platform That Perturbs Membrane Order in a Calcium-Dependent Manner. *J. Mol. Biol.* **2017**, *429* (24), 3875–3892. https://doi.org/https://doi.org/10.1016/j.jmb.2017.10.017.

(2) Lai, A. L.; Freed, J. H. SARS-CoV-2 Fusion Peptide Has a Greater Membrane Perturbating Effect than SARS-CoV with Highly Specific Dependence on Ca2+. *J. Mol. Biol.* **2021**, *433* (10), 166946. https://doi.org/https://doi.org/10.1016/j.jmb.2021.166946.

(3) Studier, F. W. Protein Production by Auto-Induction in High Density Shaking Cultures. *Protein Expr Purif* **2005**, *41* (1), 207–234.

(4) Belouzard, S.; Millet, J. K.; Licitra, B. N.; Whittaker, G. R. Mechanisms of Coronavirus Cell Entry Mediated by the Viral Spike Protein. *Viruses* **2012**, *4* (6), 1011–1033. https://doi.org/10.3390/v4061011.

(5) Han, X.; Tamm, L. K. A Host-Guest System to Study Structure-Function Relationships of Membrane Fusion Peptides. *Proc. Natl. Acad. Sci. U. S. A.* **2000**, *97* (24), 13097–13102. https://doi.org/10.1073/pnas.230212097.

(6) Glover, K. J.; Whiles, J. A.; Wu, G.; Yu, N.; Deems, R.; Struppe, J. O.; Stark, R. E.; Komives, E. A.; Vold, R. R. Structural Evaluation of Phospholipid Bicelles for Solution-State Studies of Membrane-Associated Biomolecules. *Biophys J* **2001**, *81* (4), 2163–2171. https://doi.org/http://dx.doi.org/10.1016/S0006-3495(01)75864-X.

(7) Piai, A.; Fu, Q.; Dev, J.; Chou, J. J. Optimal Bicelle Size q for Solution NMR Studies of the Protein Transmembrane Partition. *Chem. – A Eur. J.* **2017**, *23* (6), 1361–1367. https://doi.org/10.1002/chem.201604206.

(8) Caldwell, T. A.; Baoukina, S.; Brock, A. T.; Oliver, R. C.; Root, K. T.; Krueger, J. K.; Glover, K. J.; Tieleman, D. P.; Columbus, L. Low-q Bicelles Are Mixed Micelles. *J. Phys. Chem. Lett.* **2018**, *9* (15), 4469–4473. https://doi.org/10.1021/acs.jpclett.8b02079.

(9) Lu, Z.; Van Horn, W. D.; Chen, J.; Mathew, S.; Zent, R.; Sanders, C. R. Bicelles at Low Concentrations. *Mol Pharm* **2012**, *9* (4), 752–761. https://doi.org/10.1021/mp2004687.

(10) and, V. A. J.; Orekhov*, V. Y. Targeted Acquisition for Real-Time NMR Spectroscopy. **2006**. https://doi.org/10.1021/JA062146P.

(11) Jaravine, V.; Ibraghimov, I.; Yu Orekhov, V. Removal of a Time Barrier for High-Resolution Multidimensional NMR Spectroscopy. *Nat. Methods* **2006**, *3* (8), 605–607. https://doi.org/10.1038/nmeth900.

(12) Kazimierczuk, K.; Orekhov, V. Y. Accelerated NMR Spectroscopy by Using Compressed Sensing. *Angew. Chemie Int. Ed.* **2011**, *50* (24), 5556–5559. https://doi.org/10.1002/anie.201100370.

(13) Orekhov, V. Y.; Jaravine, V. A. Analysis of Non-Uniformly Sampled Spectra with Multi-Dimensional Decomposition. *Prog. Nucl. Magn. Reson. Spectrosc.* **2011**, *59* (3), 271–292. https://doi.org/10.1016/J.PNMRS.2011.02.002.

(14) Bax, A.; Grzesiek, S. No Title. *Acc. Chem. Res.* **1993**, *26*, 131.

(15) Eletsky, A.; Kienhofer, A.; Pervushin, K. TROSY NMR with Partially Deuterated Proteins. *J Biomol NMR* **2001**, *20* (2), 177–180.

(16) Salzmann, M.; Wider, G.; Pervushin, K.; Senn, H.; Wüthrich, K. TROSY-Type Triple-Resonance Experiments for Sequential NMR Assignments of Large Proteins. *J. Am. Chem. Soc.* **1999**, *121*, 844–848.

(17) Carlomagno, T.; Maurer, M.; Sattler, M.; Schwendinger, M. G.; Glaser, S. J.; Griesinger, C. PLUSH TACSY: Homonuclear Planar TACSY with Two-Band Selective Shaped Pulses Applied to C(Alpha),C' Transfer and C (Beta),C (Aromatic) Correlations. *J Biomol NMR* **1996**, *8* (2), 161–170. https://doi.org/10.1007/BF00211162.

(18) Montelione, T. G.; Lyons, A. B.; Emerson, S. D.; Tashiro, M. An Efficient Triple Resonance Experiment Using Carbon-13 Isotropic Mixing for Determining Sequence-Specific Resonance Assignments of Isotropically-Enriched Proteins. *J. Am. Chem. Soc.* **1992**, *114*, 10974–10975.

(19) Peti, W.; Griesinger, C.; Bermel, W. Adiabatic TOCSY for C,C and H,H J-Transfer. *J Biomol NMR* **2000**, *18* (3), 199–205.

(20) Yamazaki, T.; Foreman-Kay, D. J.; Kay, E. L. Two-Dimensional NMR Experiments for Correlating 13CB and 1H Chemical Shifts of Aromatic Residues in 13C-Labeled Proteins via Scalar Couplings. *J. Am. Chem. Soc.* **1993**, *115*, 11054–11055.

(21) Eichmüller, C.; Schüler, W.; Konrat, R.; Kräutler, B. Simultaneous Measurement of Intra- and Intermolecular NOEs in Differentially Labeled Protein-Ligand Complexes*. *J. Biomol. NMR* **2001**, *21* (2), 107–116. https://doi.org/10.1023/A:1012480532569.

(22) Pervushin, K.; Riek, R.; Wider, G.; Wüthrich, K. Transverse Relaxation-Optimized Spectroscopy (TROSY) for NMR Studies of Aromatic Spin Systems in 13C-Labeled Proteins. *J. Am. Chem. Soc.* **1998**, *120* (25), 6394–6400. https://doi.org/10.1021/ja980742g.

(23) Marsh, J. A.; Singh, V. K.; Jia, Z.; Forman-Kay, J. D. Sensitivity of Secondary Structure Propensities to Sequence Differences between Alpha- and Gamma-Synuclein: Implications for Fibrillation. *Protein Sci* **2006**, *15* (12), 2795–2804. https://doi.org/ps.062465306 [pii] 10.1110/ps.062465306.

(24) Peng, J. W.; Wagner, G. Mapping of Spectral Density Functions Using Heteronuclear NMR Relaxation Measurements. *J. Magn. Reson.* **1992**, *98*, 308–332.

(25) Peng, J. W.; Wagner, G. Frequency Spectrum of NH Bonds in Eglin C from Spectral Density Mapping at Multiple Fields. *Biochemistry* **1995**, *34*, 16733–16752.

(26) Farrow, N. A.; Zhang, O.; Szabo, A.; Torchia, D. A.; Kay, L. E. Spectral Density Function Mapping Using 15N Relaxation Data Exclusively. *J. Biomol. NMR* **1995**, *6*, 153–162.

(27) Fushman, D.; Weisemann, R.; Thüring, H.; Rüterjans, H. Backbone Dynamics of Ribonuclease T1 and Its Complex with 2'GMP Studied by Two-Dimensional Heteronuclear NMR Spectroscopy. *J. Biomol. NMR* **1994**, *4*, 61–78.

(28) Aguilar, J. A.; Nilsson, M.; Bodenhausen, G.; Morris, G. A. Spin Echo NMR Spectra without J Modulation. *Chem. Commun.* **2012**, *48* (6), 811–813.

(29) Koppisetti, R. K.; Fulcher, Y. G.; Jurkevich, A.; Prior, S. H.; Xu, J.; Lenoir, M.; Overduin, M.; Van Doren, S. R. Ambidextrous Binding of Cell and Membrane Bilayers by Soluble Matrix Metalloproteinase-12. *Nat. Commun.* **2014**, *5*. https://doi.org/10.1038/ncomms6552.

(30) Xu, C.; Wang, Y.; Liu, C.; Zhang, C.; Han, W.; Hong, X.; Wang, Y.; Hong, Q.; Wang, S.; Zhao, Q.; Wang, Y.; Yang, Y.; Chen, K.; Zheng, W.; Kong, L.; Wang, F.; Zuo, Q.; Huang, Z.; Cong, Y. Conformational Dynamics of SARS-CoV-2 Trimeric Spike Glycoprotein in Complex with Receptor ACE2 Revealed by Cryo-EM. *Sci. Adv.* **2021**, *7* (1). https://doi.org/10.1126/sciadv.abe5575.

(31) Cai, Y.; Zhang, J.; Xiao, T.; Peng, H.; Sterling, S. M.; Walsh, R. M.; Rawson, S.; Rits-Volloch, S.; Chen, B. Distinct Conformational States of SARS-CoV-2 Spike Protein. *Science (80-.).* **2020**, *369* (6511), 1586–1592. https://doi.org/10.1126/science.abd4251.

(32) Zhou, T.; Tsybovsky, Y.; Gorman, J.; Rapp, M.; Cerutti, G.; Chuang, G.-Y.; Katsamba, P. S.; Sampson, J. M.; Schön, A.; Bimela, J.; Boyington, J. C.; Nazzari, A.; Olia, A. S.; Shi, W.; Sastry, M.; Stephens, T.; Stuckey, J.; Teng, I.-T.; Wang, P.; Wang, S.; Zhang, B.; Friesner, R. A.; Ho, D. D.; Mascola, J. R.; Shapiro, L.; Kwong, P. D. Cryo-EM Structures of SARS-CoV-2 Spike without and with ACE2 Reveal a PH-Dependent Switch to Mediate Endosomal Positioning of Receptor-Binding Domains. *Cell Host Microbe* **2020**, *28* (6), 867-879.e5. https://doi.org/https://doi.org/10.1016/j.chom.2020.11.004.

(33) Hubbard, S. J.; Thornton, J. M. NACCESS 2.1.1. The University of Manchester: Manchester, UK 1996.

(34) Pervushin, K.; Braun, D.; Fernández, C.; Wüthrich, K. [15N,1H]/[13C,1H]-TROSY for Simultaneous Detection of Backbone 15N–1H, Aromatic 13C–1H and Side-Chain 15N–1H2 Correlations in Large Proteins. *J. Biomol. NMR* **2000**, *17* (3), 195–202. https://doi.org/10.1023/A:1008399320576.

(35) Laskowski, R. A.; Rullmannn, J. A.; MacArthur, M. W.; Kaptein, R.; Thornton, J. M. AQUA and PROCHECK-NMR: Programs for Checking the Quality of Protein Structures Solved by NMR. *J Biomol NMR* **1996**, *8* (4), 477–486.

(36) Williams, C. J.; Headd, J. J.; Moriarty, N. W.; Prisant, M. G.; Videau, L. L.; Deis, L. N.; Verma, V.; Keedy, D. A.; Hintze, B. J.; Chen, V. B.; Jain, S.; Lewis, S. M.; Arendall III, W. B.; Snoeyink, J.; Adams, P. D.; Lovell, S. C.; Richardson, J. S.; Richardson, D. C. MolProbity: More and Better Reference Data for Improved All-Atom Structure Validation. *Protein Sci.* **2018**, *27* (1), 293–315. https://doi.org/https://doi.org/10.1002/pro.3330.